ARTICLES

Lattice-embedded multiconfigurational self-consistent-field calculations of the Mn-perturbed *F*-center defect in CaF_2:Mn

A. C. Lewandowski* and T. M. Wilson
Computational Solid State Research Laboratory, Physics Department, Oklahoma State University, Stillwater, Oklahoma 74078
(Received 8 March 1995)

We report on the results of *ab initio* ground- and excited-state multiconfigurational self-consistent-field (SCF) embedded-cluster calculations for the Mn-perturbed *F*-center (Mn/*F*) defect in CaF_2:Mn. This defect has long played a central role in the understanding of the absorption and emission characteristics of this material following irradiation. An approximate embedding method is employed whereby the potential due to the external lattice surrounding the cluster representing the Mn/*F* defect is described by means of lattice-centered Gaussian charge distributions, the parameters of which are determined in conjunction with SCF force calculations so as to stabilize the cluster. The ground and excited many-electron state energies of spin 2 and 3 of the Mn/*F* defect were calculated using the method of complete active space SCF. These calculations show that the ground state of the Mn/*F* defect is spin 2 thus making the optical transitions spin-allowed, and accounts for the absorption oscillator strength enhancement following irradiation. The calculated excited-state levels are used to interpret the observed optical absorption spectrum. Our calculations also show that the important peak at 540 nm does not arise from transitions within the Mn/*F* defect considered in this study. This peak is possibly related to Mn-perturbed *M* centers.

I. INTRODUCTION

The optical properties of radiation-induced defects in CaF_2:Mn have been of interest since its introduction as a highly efficient thermoluminescent radiation dosimeter in 1957 by Ginther and Kirk[1] and its later adoption as the standard dosimeter material by the U.S. Navy. While CaF_2:Mn has long played an important role in radiation dosimetry,[2–7] only since 1980 have the processes of defect formation, energy storage, and release in the form of luminescence been studied in detail. Through optical absorption,[8–12] photoluminescence,[8,12–14] and thermoluminescence (TL)[1,10,12,15–17] measurements, the role Mn^{2+} plays in determining the absorption and emission characteristics of CaF_2:Mn following irradiation has begun to emerge.

Explanation of the optical absorption, TL, and photoluminescence spectra, conducted by McKeever *et al.*[11] on samples before and after irradiation and with varying Mn dopant concentrations, have centered around a proposed defect complex consisting of an *F* center adjacent to one or more substitutional Mn^{2+} ion impurities. Photoluminescence and TL studies both indicate that the optically active radiation-induced defect is Mn related with TL peaks at 200 and 550 K producing emission at 495 nm. Photoluminescence[13] and optical absorption[11] measurements have assigned this emission to the $^4T_{1g}(^4G) \rightarrow {}^6A_{1g}(^6S)$ transition of the Mn^{2+} ion. Mn^{2+} enters the lattice substitutionally and occupies sites of O_h symmetry. With the ground state as a spin sextet and the excited states as spin quartet and doublet, the optical transitions are both spin and parity forbidden. However, McKeever *et al.*,[11] using long samples with high Mn concentrations ($\sim 3\%$), were able to obtain Mn^{2+} absorption spectra for nonirradiated CaF_2:Mn. These spectra, along with the earlier photoluminescence spectra, have been successfully analyzed in terms of ligand field theory[11,13,18] and more recently by *ab initio* multiconfigurational self-consistent-field calculations.[18]

Following irradiation, the absorption exhibits the creation of new structure and an increase in oscillator strength by $\sim 10^3$.[11] This effect has been understood in terms of the proposed Mn-perturbed *F*-center model as arising from the exchange coupling involving the Mn^{2+} $3d^5$ electrons and the *F*-center electron. This enhancement, however, occurs only for samples irradiated at room temperature, indicating that the absorption enhancement requires transport perhaps to form the *F* centers adjacent to Mn^{2+} impurities.

The idea of absorption enhancement arising from the creation of 3*d*-ion *F*-center complexes following irradiation is not new. The main observations regarding the behavior of the absorption and emission spectra from Mn-doped CaF_2 before and after irradiation roughly parallel the trends observed to occur in Mn-doped $RbMgF_3$,[19,20] MgF_2,[21–23] and $KMgF_3$.[23–25] Empirical models developed for these materials attribute the enhancement of the 3*d*-ion absorption to the lifting of the spin and symmetry selection rules following irradiation. The transitions become spin allowed as a result of an exchange interaction between the *F*-center electron and the impurity 3*d* electrons.[23] These studies also show that the lifting of the spin selection rule is the dominant mechanism for the enhancement, while changes in the site symmetry do not appreciably affect the transitions.[21,22]

Given the body of evidence that has emerged over the

0163-1829/95/52(1)/100(10)/$06.00

last two decades with regard to the types of radiation-induced defect complexes responsible for optical absorption in CaF_2:Mn and given the close parallels with models proposed for Mn-doped MgF_2, $KMgF_3$, and $RbMgF_3$, a defect complex consisting of an F center perturbed by one or two Mn^{2+} substitutional impurities seems a likely candidate to account for the absorption spectrum following irradiation. With the experimental data now well established, the state of research has reached the point where quantum-mechanical calculations are needed to provide a better understanding and verification of this model.

Toward this end, we present the results of *ab initio* self-consistent-field calculations of the ground and excited states of the Mn-perturbed F-center (Mn/F) defect. The computational quantum-mechanical methods employed include restricted closed-shell Hartree-Fock (RHF), restricted open-shell Hartree-Fock (ROHF), spin-projected unrestricted Hartree-Fock (PUHF), spin-projected unrestricted Møller-Plesset many-body perturbation theory to second order (PUMP2), and complete active space self-consistent-field (CASSCF) calculations. All of these methods have been implemented for d electrons in the GAUSSIAN 92 (Ref. 26) general purpose quantum-chemical program. These methods will be applied to clusters in the presence of an embedding external arrangement of charge. This is aided by capabilities in GAUSSIAN 92 that permit the inclusion into the Fock operator terms which reflect the distribution of either external point ions or external Gaussian charge distributions.

II. THEORETICAL MODEL

A. The embedded Mn-perturbed F-center cluster

In Fig. 1 is shown the geometry of the Mn-perturbed F-center cluster, $[MnCa_3F_6Vac]^{1+}$, we use to model the proposed defect created in CaF_2:Mn following irradiation. Several reviews of experimental investigations and theoretical *ab initio* calculations show that the F center is strongly coupled to the host lattice with its transition energies easily shifted by neighboring defects.[27–30] This defect involves an electron trapped in a vacancy represented by diffuse electronic states and so will be sensitive to changes in the external field due to the surrounding crystal lattice.[29,30] As a consequence, a major part of this study involved the development of a semiclassical embedding method whereby the external crystal lattice is represented by a finite arrangement of charge. The cluster depicted in Fig. 1 shows only that portion of the crystal treated quantum mechanically with the remaining surrounding lattice treated classically in the final calculations.

The cluster embedding procedure employed in these calculations is described in detail elsewhere.[31] Briefly stated, the method involves initially embedding (i.e., stabilizing) the nondefective $[Ca_4F_7]^{1+}$, $S=0$ cluster shown in Fig. 2. This is done by representing the external CaF_2 lattice as a collection of lattice-centered Gaussians characterized by different charges and Gaussian exponents (q_F,α_F) and (q_{Ca},α_{Ca}). Through an iterative scheme consisting of SCF force calculations and adjustments of the external Gaussian parameters, the net forces on the cluster ions can be brought to zero. In this fashion, an effective external Coulombic field is produced in the quantum cluster region so as to exactly balance the quantum-mechanical forces on the cluster ions and simultaneously account for the fact that the external charge distribution is finite. The interactions within this distribution contribute to the overall energy of the system and are treated classically.

With the nondefective cluster stabilized, the F-center cluster, $[Ca_4F_6Vac]^{1+}$, $S=\frac{1}{2}$, is created by the removal of the center F^- ion and the addition of an electron. The replacement of the central F^- ion by an F center leads to an imbalance of the forces on the outer Ca^{2+} and F^- ions; hence the locations of these ions must be relaxed to

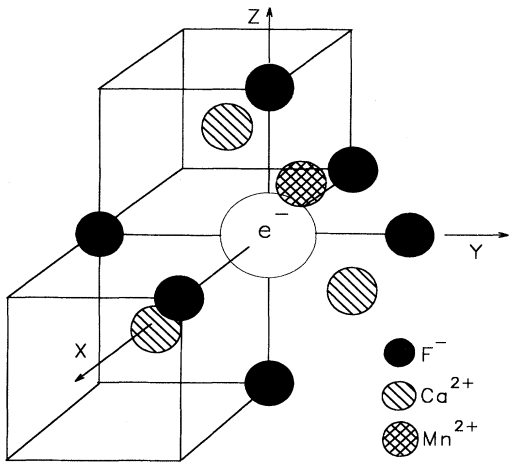

FIG. 1. Diagram of the Mn-perturbed F-center cluster, $[MnCa_3F_6Vac]^{1+}$, used to model the defect created in CaF_2:Mn following irradiation. After embedding and following relaxation, the vacancy-F and vacancy-Mn(Ca) distances are 2.70 and 2.29 Å, respectively.

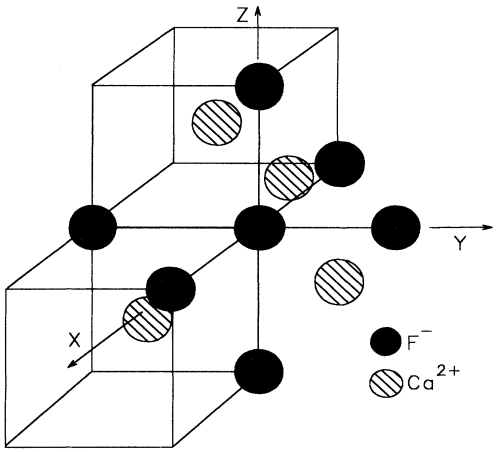

FIG. 2. Diagram of the nondefective cluster, $[Ca_4F_7]^{1+}$. The ions are arranged at the experimental Ca-F distance of 2.366 Å (Ref. 27). SCF calculations based on this cluster are used to determine the embedding lattice parameters.

new equilibrium positions. The parameters of the external charge distribution are held constant throughout this relaxation. In the relaxed geometry the vacancy-F distance is 2.70 Å and the vacancy-Ca distance is 2.29 Å. This represents a 1.2% inward relaxation for the F^- ions and a 3.3% inward relaxation for the nearest-neighbor Ca^{2+} ions. The magnitude and direction of these relaxations appear reasonable in view of recent calculations involving the relaxation of F-center defects in other ionic crystals by Vail and Woodward using the ICECAP program.[32] They describe an embedded F center in NaF for which they find a 5% inward relaxation of the nearest-neighbor Na^+ ions.

This cluster has been used with some degree of success in semiempirical and multiple scattering $X\alpha$ studies of the electronic structure of the F center in CaF_2.[27,33] Since the energy levels of an F center can be easily shifted by changes in the site symmetry and due to the size of the overlap of the F-center wave functions with the first-nearest-neighbor and second-nearest-neighbor ions, this particular choice of cluster is based on the need to completely surround the vacancy by quantum-mechanical ions. Furthermore, since the external charge is arranged symmetrically about the origin, locating the vacancy at the origin reduces the possibility of introducing artificial distortions in the vacancy electronic charge distribution that would arise due to the finite extension of the external classical charge distribution.

The embedded Mn-perturbed F-center cluster, $[MnCa_3F_6Vac]^{1+}$, is formed by replacing one of the Ca^{2+} ions by a Mn^{2+} ion. As indicated in Fig. 1, the Mn^{2+} ion is located adjacent to three quantum-mechanical F^- ions and the vacancy containing the F-center electron (which is treated quantum mechanically by locating basis functions at the origin). The cluster has C_{3v} symmetry. The other four nearest-neighbor fluorine atoms to the Mn^{2+} are external to the cluster and are represented by lattice-centered Gaussians. It is therefore necessary to determine what effect this would have on the d-to-d transitions. Test calculations on the $[MnCa_3F_7]^{1+}$ cluster (that is, Fig. 1 with the central vacancy replaced by a F^- ion) show that the ground-state to first excited-state transition energy does not vary significantly (<0.1 eV) from the analogous ($^6A_{1g}(^6S)\rightarrow{}^4T_{1g}(^4G)$) transition for O_h eight-coordinated Mn^{2+}.[18] This must in part be due to the localized nature of the $3d$ electrons that give rise to these excited states and the use of Gaussians for describing the ions external to the cluster. Alternatively, our attempts to replace a fluorine by an F center in the embedded $[MnF_8]^{6-}$ cluster (used to describe the electronic structure of the isolated centrally located substitutional Mn^{2+} impurity[18]) proved unsuccessful due to the inability to confine the F-center electron within the cluster region. This shows the importance of placing the F center at the center of the cluster. Finally, we note that, from a practical standpoint, the size of the quantum cluster is limited to that for which the CASSCF method can be used to calculate the excited states. Thus, the Mn-perturbed F-center cluster in Fig. 1 was chosen to represent the Mn/F defect as it adequately embeds the F center, it has the correct symmetry of the defect, and it allows for the treatment of the important exchange interaction between the F center and the manganese impurity.

B. Choice of basis

The choice of a variational basis set is perhaps the most important consideration when attempting to perform accurate SCF calculations for many-electron systems. One attempts to choose a basis set that, while limited enough in size for practical calculations, is also flexible enough so as to not unduly bias the results. Basis-set-related errors have been reviewed in the literature.[34] The standard Gaussian basis sets for the F^- ion and Ca atom tabulated by Huzinaga *et al.*[35] for use in molecular calculations provide a good starting point. The basis functions listed in these tables, while adequate for atomic calculations, must be augmented by the addition of more diffuse s, p, and d Gaussian atomic basis functions for molecular calculations. In total, 9 atomic basis functions were used for fluorine and 13 for calcium with the contraction patterns F(4,3,2/4,3) and Ca(4,3,3,2/4,3,2). The basis set for the Mn^{2+} ion consisted of 23 atomic basis functions with the (4,3,3,2/4,3,2/4,3) contraction pattern and was taken from a detailed analysis of the $[MnF_8]^{6-}$ cluster used to calculate the electronic states of the isolated manganese impurity in CaF_2.[18]

In these calculations, vacancy-centered basis functions are used to model the electronic charge distribution within the vacancy. Figure 3 shows the square of the four s-type and six p-type vacancy-centered uncontracted Gaussian basis functions that were chosen to physically occupy most of the vacancy region. The Gaussian exponents are displayed in the figure.

Once the ground state has been obtained with this initial basis, and before embedding the cluster, the next step is to optimize the basis set. The basis set is optimized by varying the Gaussian exponential scale factors so as to minimize the ground-state energy. For practical reasons, this variation is performed at the Hartree-Fock level of

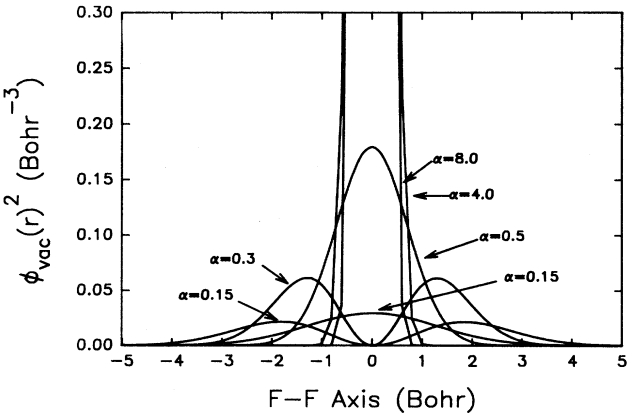

FIG. 3. Square of the Gaussian basis functions arrayed about the vacancy site situated at the origin. Consisting of four s-type and six p-type uncontracted Gaussian functions, this basis is used to model the electronic charge within the vacancy region.

theory and only for basis functions representing the valence electrons. We found that this variation works best for the cluster in isolation. Attempting to vary the valence basis functions in the presence of an external charge distribution tends to produce basis functions so extended that a significant amount of charge accumulates in the region of the external lattice-centered Gaussians. The charge has, in effect, exited the quantum cluster. This is an example of the spurious tunneling effect observed by Kunz and Vail for other systems.[36]

C. CASSCF active space

The idea of merging configuration interaction (CI) and SCF (known as multiconfigurational self-consistent field, or MCSCF) goes back to the early days of quantum chemistry[37] and has since seen a substantial development in terms of its theoretical basis and computational implementation.[38–45] The goal of CASSCF is to provide an adequate description of the electronic structure with a relatively compact wave function. This is achieved by constructing a multiconfigurational wave function from a selected subset of orbitals and by a simultaneous variational optimization of the orbitals and the configurational coefficients. This method is more feasible than a large CI calculation and more accurate than a truncated CI expansion where the orbitals are frozen according to some criterion, e.g., canonical Hartree-Fock orbitals or natural orbitals. In the CASSCF method the orbitals can change shape within the given configurations; thus CASSCF is more powerful than CI in describing the polarization of the electronic cloud caused by an external field. In addition, CASSCF is analogous to CI in that it can calculate upper bounds to the total energy many-electron excited states of the same spin and spatial symmetry as the ground state.[46,47] The difference is that for CASSCF the orbitals may be optimized for each excited root. For this reason CASSCF is a powerful computational tool for the calculation of a system's multiplet structure. It is especially useful for low symmetry situations for which ground-state methods, such as Hartree-Fock and many-body perturbation theories, cannot be applied to the study of the excited states of a given spatial and spin symmetry.

The Mn-perturbed *F*-center defect shown in Fig. 1 has an overall charge of $+1$. Each F^- ion has closed $2p$ shells and each Ca^{2+} has closed $3p$ shells. The Mn^{2+} has a $3d^5$ configuration outside closed shells and, in addition, there is a single electron described by the *s*- and *p*-like atomic basis functions in the vacancy. Given this arrangement, we consider the $S=2$ and $S=3$ spin configurations and construct the two active spaces as indicated by the diagrams in Fig. 4. The CASSCF method as implemented in GAUSSIAN 92 is a spin-restricted procedure so that the orbitals represented in Fig. 4 have the same spatial dependencies regardless of spin.

Within the CASSCF scheme the spin-2 or spin-3 ground and excited states are represented by wave functions which are linear combinations of determinants corresponding to all possible arrangements of electrons over the molecular orbitals in the spin-2 or spin-3 active

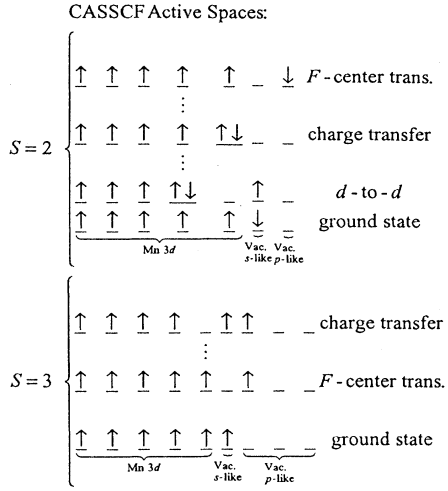

FIG. 4. Diagrams indicating the CASSCF active spaces used to calculate the spin-2 and -3 ground and excited states of the Mn-perturbed *F*-center cluster.

spaces. For instance, the *n*th state of spin 2 is represented by a wave function that is in a linear combination of *all* configurations allowed within the spin-2 active space. CASSCF differs from CI in that *both* the linear coefficients and the molecular orbitals are optimized for the *n*th state.

The spin-3 configuration consists of the five Mn^{2+} $3d^5$ electrons spin aligned with the vacancy electron parallel to these. The CASSCF active space for this spin is then formed from the five Mn^{2+} $3d$-like, the vacancy *s*-like, and the three vacancy *p*-like molecular orbitals. This choice gives a total of 84 spin-3 configurations. With reference to Fig. 4 we can identify three classes of spin-3 configurations in increasing energy. The ground state consists of occupied Mn^{2+} $3d$-like and vacancy *s*-like molecular orbitals. The first excited configurations involve excitations within the vacancy into the vacancy *p*-like molecular orbitals. These are denoted in Fig. 4 as spin-3 *F*-center transitions. The final set of excited spin-3 configurations represent Mn-to-vacancy charge transfer transitions. These are expected to be highly energetic since they require a transfer of an electron off the Mn to doubly occupy the vacancy. Nevertheless, these are included in the formation of the multiconfigurational states to add variational flexibility. The possibility of including in the CASSCF active space Ca^{2+} or F^- molecular orbitals to describe charge transfer states involving these ions was rejected on the grounds that they were not found to play a significant role in the *d*-to-*d* transitions of the isolated Mn^{2+} impurity,[18] and would significantly increase the number of configurations.

A different active space was used for the spin-2 configurations. For these configurations one electron is antiparallel to the majority spin so that the possibility of double *d*-like molecular orbital occupations greatly increases the number of allowed spin-2 arrangements. To reduce the number of determinants in the CASSCF ex-

pansion and the overall size of the spin-2 excited-state calculations, this active space was restricted to include only one vacancy p-like molecular orbital as shown in Fig. 4. We note that while this reduction in the active space reduces the variational flexibility, the CASSCF method varies both the expansion coefficients and the molecular orbitals. Thus the single p-like molecular orbital could still take on suitable p_x, p_y, or p_z character or linear combinations thereof as required to best represent the particular excited state. Nevertheless, this choice still results in there being a total of 140 spin-2 configurations.

With reference to Fig. 4, the ground state of spin 2 consists of all five Mn^{2+} $3d^5$ molecular orbitals occupied and spin aligned. The vacancy electron is antiparallel to these. This arrangement will produce the spin-2 ground state since each electron occupies a different spatial orbital and hence the Coulomb repulsion is minimized. Higher in energy will be a manifold of states consisting of linear combinations of determinants representing different occupancies of the five d-like and vacancy molecular orbitals. These can be conveniently categorized as spin-2 d-to-d, charge transfer, and F-center transitions. The d-to-d transitions consist of the various double occupancies of the Mn^{2+} $3d$ molecular orbitals with the spin of the vacancy electron aligned with the majority spin. The charge transfer transitions signify the transfer of the electron out of the vacancy and onto the Mn^{2+} ion to form a Mn^{1+} $3d^6$ configuration. The F-center transitions involve excitations from the s-like molecular orbital into the more excited vacancy p-like molecular orbitals within the vacancy.

Since the wave functions are multiconfigurational, the states of a given spin will themselves be represented as linear combinations of these different categories; however, very often one of the categories will dominate and the multiconfigurational wave function can be assigned a specific character (i.e., a particular excited state could be categorized as being due mainly to a d-to-d transition or an F-center transition, etc.) This in turn will allow for a physical interpretation of the various experimental spectrum peaks.

III. EXCITED-STATE CALCULATIONS

The calculations begin with PUHF results obtained for the ground states of spin 2 and 3. All the calculations were performed in the presence of the embedding external charge distribution established for this cluster in the previous sections. At the PUHF level of theory the spin-3 ground state lies 0.11 eV *above* the spin-2 ground state. To test this ordering of levels, PUMP2 calculations show an increase in this separation with the spin-3 ground state lying 0.17 eV above the spin-2 ground state. This particular ordering of the ground states will play an important role in the understanding of the optical spectrum for irradiated CaF_2:Mn.

Since CASSCF in GAUSSIAN 92 is a spin-restricted procedure, spin-2 and -3 ROHF ground states were obtained to establish the initial orbitals for the active spaces. With these ROHF starting orbitals, successive CASSCF calculations were performed within the spin-2 and -3 manifolds. Since the Hylleraas-Undheim theorem[46,47] guarantees that each root will be a rigorous upper bound to the actual excited-state energy, optimizing the orbitals so as to minimize the value of a selected root will produce the lowest possible upper bound of the selected excited-state energy for the given active space and basis set. By incrementing the root for which the orbitals are optimized for each successive CASSCF calculation, an energy level spectrum is produced. Table I summarizes the results for the spin-2 manifold of states. What is listed are the transition energies from the spin-2 CASSCF ground state into the spin-2 CASSCF excited states. Transitions involving a change in spin are not listed, as these would produce negligible absorption compared to the spin-allowed transitions. We emphasize that the excited-state energies calculated in this manner are many-electron state energies and not one-electron energies. The second column of this table lists the absolute transition energies and the third column lists these transition energies after a rigid shift of -0.647 eV applied only to the excited states dominated by configurations representing d-to-d transitions. The fourth column lists these transition energies converted into wavelength. Figure 5 displays the results of Table I graphically. In addition, Fig. 5 displays the spin-3

TABLE I. Spin-2 CASSCF transition energies for the embedded Mn-perturbed F-center cluster. Each root represents a separate CASSCF calculation with the orbitals optimized for that particular root. The transition energies are calculated with respect to the spin-2 CASSCF ground state.

Root	G.S.→E.S. Trans. Energy (eV)	After rigid shift of -0.647 eV (eV)[a]	Wavelength (nm)
2	3.445	2.798	441
3	3.604	2.957	417
4	3.665	3.018	409
5	3.719	3.072	402
6	3.760	3.113	396
7	3.855	3.208	385
8	3.881	3.234	382
9	3.885	3.238	381
10	3.909	3.263	378
11	4.263	3.616	341
12	4.302	3.655	338
13	4.503	3.856	320
14	4.582	3.935	314
15	4.620	3.973	310
16	4.703	4.056	304
17	4.756	4.109	300
18	4.788	4.141	298
19	5.423	4.776	258
20	5.788	5.141	240
21	6.018	5.371	230
22	6.132	5.485	225
23	6.171	5.524	223
24	6.425		192
25	6.477		190

[a]Applied to all roots except 24 and 25 which correspond to F-center transitions.

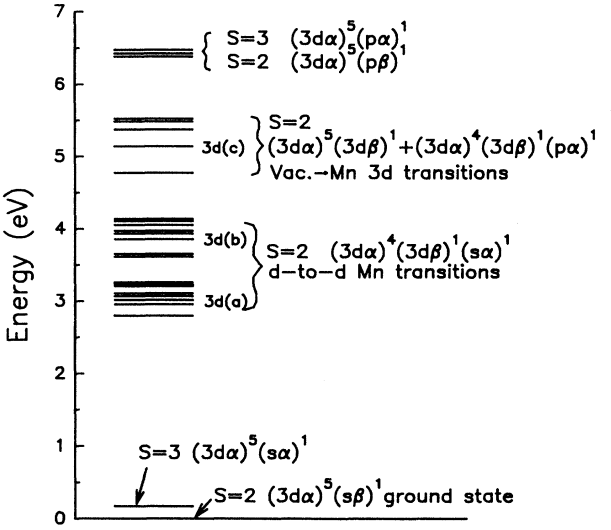

FIG. 5. The CASSCF energy levels for the Mn-perturbed *F*-center cluster relative to the spin-2 ground state. This is essentially a graphical representation of column 3 of Table I. Also displayed, relative to the spin-2 ground state, are the spin-3 ground and first excited states. The states are categorized according to the dominant configurations in the multiconfiguration expansions.

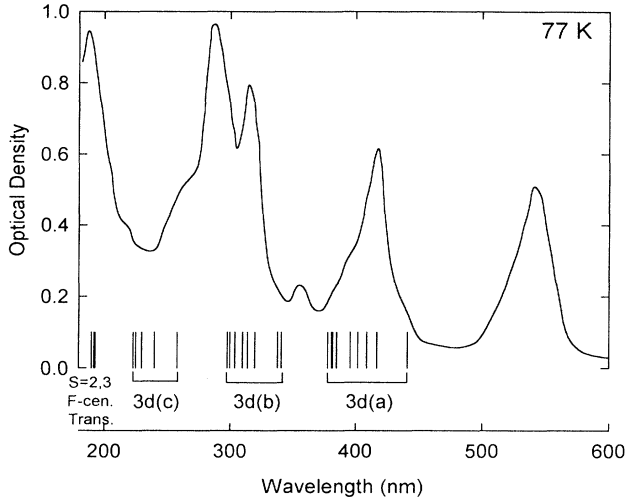

FIG. 6. Overlay of the CASSCF transition energies with the optical absorption data of McKeever *et al.* (Ref. 11) for CaF_2:Mn (3%). The data was recorded at 77 K following 367 Gy γ irradiation at room temperature. Displayed are the calculated spin-2 ground- to excited-state transitions and the single spin-3 ground- to excited-state transition.

ground state and first excited state located approximately 0.2 and 6.5 eV above the spin-2 ground state, respectively. Figure 6 displays all the calculated spin-2 and -3 transitions on an overlay with the experimental optical spectrum obtained by McKeever *et al.*[11]

The spin-3 ground- to first-excited-state transition energy was calculated to occur at approximately 193 nm and corresponds to a spin-3 *F*-center transition. Note that since the spin-3 first excited state does not correspond to a *d*-to-*d* transition, this state is not subject to the -0.647 eV rigid shift. Since further spin-3 excited states will occur at higher energies and would thus place them outside the spectral range of the experimental optical data, higher states of this spin were not considered in this study.

The application of a -0.647 eV rigid shift for the *d*-to-*d* transitions stems from the fact that for *d* electrons CASSCF does a much better job predicting the *relative* spacing of the *d*-to-*d* energy levels within a given spin manifold than it does in predicting the absolute transition energies. From a previous CASSCF analysis of the $[MnF_8]^{6-}$ cluster, the -0.647 eV rigid shift was introduced so as to bring the calculated spectrum into alignment with the experimentally determined spectrum.[18] Since the basis set employed about the Mn^{2+} ion for this study is identical to that of the Mn^{2+} ion for the $[MnF_8]^{6-}$ cluster, this same -0.647 eV rigid shift is adopted for the *d*-to-*d* transitions occurring within the Mn-perturbed *F*-center cluster. The optical absorption spectrum arising from the isolated manganese defect in unirradiated CaF_2:Mn is well defined with the spectrum peaks established as resulting from specific Mn^{2+} $3d^5$ *d*-to-*d* transitions.[11,18] As a result, it was possible to determine an accurate value of the rigid shift for that system while it is not possible for the present Mn-perturbed *F*-center system since the spectrum is not as fully characterized. Thus, in order to avoid a completely *ad hoc* rigid shifting of the CASSCF levels, the -0.647 eV rigid shift was applied only to excited states resulting from *d*-to-*d* transitions.

The details as to the origin and justification of this rigid shift are discussed in previous work.[18] Essentially, this energy is closely related to the correlation energy corrections employed by Richardson and Janssen[48] in their analysis of the Mn center in ZnS:Mn and by Flórez, Seijo, and Pueyo[49] in their analysis of the $[MnF_6]^{4-}$ complex *in vacuo* and in the $RbMnF_3$ lattice. As discussed by these authors, the correlation energy corrections arise from atomic differential correlation effects for the $3d^5$ states of the free Mn^{2+} ion.

IV. RESULTS AND DISCUSSION

A. Relevant experimental observations

In this section we shall explain, as far as possible, the optical absorption spectrum of CaF_2:Mn following irradiation at room temperature. We begin with a brief review of some relevant experimental observations.

Figure 6 shows the optical absorption spectrum of CaF_2:Mn at 77 K following room-temperature irradiation. With reference to this figure, the most important experimental results to be explained in this paper are the following:[11] (1) the spectrum is enhanced by over two orders of magnitude following irradiation at room temperature, (2) a peak at approximatley 540 nm appears follow-

ing irradiation, and (3) this peak decays with thermal treatment along with the shorter wavelength peaks. As the sample is heated above room temperature the spectrum in Fig. 6 is observed to decay. This decay is not continuous but contains a step at approximately 525 K which is accompanied by the production of TL with emission at 495 nm. All the absorption peaks decay together at 525 K including the 540 nm peak. This implies that all the peaks are due to the same type of defect. According to the proposed TL models, the thermally released energy is transferred to a Mn-*F*-center impurity complex[11,12,50] resulting in the 495 nm TL emission. This 495 nm emission is the same wavelength observed in photoluminescence studies before irradiation and has already been confirmed as being due to the first excited state to ground state transition in Mn^{2+}. Thus, it follows that the lower-energy 540 nm peak cannot be due to Mn^{2+} absorption. The question then arises as to why the 540 nm peak and the Mn-related absorption peaks decay simultaneously. In the following two subsections, we present plausible explanations for the absorption enhancement, and the appearance and behavior of the 540 nm peak, based upon the results of our calculations.

B. Mn^{2+} absorption enhancement and structure

It has been proposed by McKeever *et al.*[11] that gamma radiation at room temperature creates *F* centers which migrate and become trapped adjacent to Mn impurities forming Mn/*F* defects which are stable at room temperature. It appears that the presence of Mn is required to stabilize the *F* centers since the *F*-center production efficiency in undoped CaF_2 is quite low.[51] With regard to the increase in the absorption spectra following irradiation, PUHF and PUMP2 calculations show that the ground state for this system in spin 2. *Therefore, the excited states corresponding to spin-2 d-to-d transitions, which are spin forbidden in the isolated Mn center, become spin allowed for the Mn-perturbed F center.* The lifting of this spin selection rule opens up a large number of spin-allowed *d*-to-*d* transitions which our calculations show lie in the 225 to 441 nm spectral range. The addition of the vacancy electron also leads to the creation of a larger number of nondegenerate states with the same spin as the ground state due to the reduction in symmetry from O_h to C_{3v}. In addition, new states arise relating to transitions within the vacancy such as the spin-2 *F*-center excited states shown in Fig. 5, giving rise to transitions at approximately 191 nm. Generally speaking, these features taken together are responsible for both the enhancement of the absorption and the increase in the complexity of the spectrum.

Figures 5 and 6 display quantitatively the results of our calculations for the Mn/*F* defect. In Fig. 5 the ground state is shown to be spin 2 with five spin-up Mn^{2+} *d* electrons and a spin-down *s*-like vacancy electron. The next highest state is spin 3, where the vacancy electron is spin aligned with the Mn^{2+} *d* electrons. PUMP2 calculations show that this level lies approximately 0.17 eV above the ground state. The next set of excited states are spin 2 and arise from Mn^{2+} *d*-to-*d* transitions. These states tend to fall into three groups which we denote 3*d*(a), 3*d*(b), and 3*d*(c). Previous CASSCF calculations obtained for the $[MnF_8]^{6-}$ O_h cluster also show a three-group structure for the *d*-to-*d* transitions over approximately the same energy ranges.[18] We conclude, therefore, that the perturbation of the Mn^{2+} by the adjacent *F* center does little to change the energetics of the internal *d*-to-*d* transitions. Instead, the major effect of the interaction with the *F*-center electron is to produce a spin-2 ground state that makes the transitions from the ground state to the three groups of *d* levels of the Mn/*F* defect spin allowed.

Groups 3*d*(a) and 3*d*(b) are dominated by linear combinations of configurations for which the spin-down electron occupies a Mn^{2+} 3*d* molecular orbital with the vacancy electron spin-up in an *s*-like molecular orbital. Our calculations show that group 3*d*(a) is responsible for transitions in the 378 to 441 nm spectral range and corresponds closely to an observed absorption peak over this same interval. The origin of this absorption band, centered in the 425 nm region, has been unclear for some time. Alcalá *et al.*[8] and Chakrabart *et al.*[50] suggest that the absorption in this region may be due to Mn^{+} centers; however, our calculations show that the 425 nm band is the result of Mn^{2+} spin-allowed *d*-to-*d* transitions, where the *F*-center electron remains localized within the vacancy.

The 3*d*(b) group of levels extends from the 298 to 341 nm range and corresponds roughly to two peaks at approximately 300 and 325 nm. This is in agreement with the conclusions reached by Chakrabarti *et al.*,[50] who assign absorption in this region to the Mn/*F* defect based on the results of thermal annealing and UV phototransfer studies. A small peak at approximately 360 nm cannot be unambiguously assigned to levels within the 3*d*(b) group and may not be related to the Mn/*F* defect. We note that the *F* band in irradiated undoped CaF_2 occurs at 376 nm.[27] Thus, this peak may be due to *F* centers not associated with manganese impurities.

The last group of levels associated with *d*-to-*d* transitions is a group we denote 3*d*(c). Unlike the previous two groups, this contains a large admixture of vacancy *p*-like molecular orbitals and, to a lesser extent, configurations representing an empty vacancy and a Mn^{+} $3d^6$ arrangement. Physically, the states in this group show a distortion of the vacancy electron charge cloud toward the Mn^{2+} ion. The levels of this group are calculated to lie in the 225 to 258 nm range and do not appear to align with any clearly distinguishable peak structure. This group of states appear to be more sensitive to the approximations inherent in these calculations than are the 3*d*(a) or 3*d*(b) groups. These approximations include the size and nature of the CASSCF active space, the imposition of a single numerical rigid shifting factor, and the inclusion of the four "outer" manganese 1nn fluorines in the external lattice. Since configurations representing the transfer of the electron out of the vacancy and onto the Mn^{2+} ion show up as important contributions for the 3*d*(c) excited states, a better representation could be obtained by inclusion into the CASSCF active space adjacent F^{-} *p*-like molecular orbitals. This would build in, to a greater extent, *interionic* correlation effects. The single

numerical rigid shifting factor of -0.647 eV, that was applied equally to the $3d$(a), $3d$(b), and $3d$(c) groups, represents an approximate *intraionic* correlation energy correction as discussed in Sec. III. The application of this rigid shift to the CASSCF results for the $[MnF_8]^{6-}$ O_h cluster representing the isolated Mn^{2+} impurity[18] brought the calculated transition energies corresponding to the $3d$(a,b) groups shown in Fig. 5 into excellent agreement with those observed experimentally. However, the application of this correction to the energy levels of the higher-lying $^4A_{2g}(^4F)$, $^4T_{2g}(^4F)$, and $^4T_{1g}(^4F)$ states results in the calculated transition energies being ~ 0.5 eV greater than the experimental values. This is largely due to the explicit neglect of charge-transfer configurations in the construction of the active space used for the CASSCF calculations. These states are primarily responsible for the $3d$(c) group of transitions shown in Fig. 5. Thus, it is to be expected that this factor should be less suitable for the $3d$(c) group where these charge-transfer configurations appear to be of equal importance. Although the active space here is much larger than that employed in the isolated Mn^{2+} impurity calculations, the inclusion into the CASSCF active space adjacent F^- p-like molecular orbitals was not made here due to the already large size of the active space (140 configurations) and the fact that four of the Mn^{2+} nearest-neighbor fluorines are included in the external lattice.

Given these considerations, it is reasonable to assume that the levels of the $3d$(c) group could be lowered to such an extent (~ 0.5 eV) that they would align with the observed structure in the 250 to 290 nm range. Our assertion that the structure in this range is related to a distortion of the electron out of the vacancy and toward the Mn is further supported by the optically stimulated luminescence measurements of Allen and McKeever.[12] These measurements show that when irradiated CaF_2:Mn is stimulated with light near 290 nm it emits luminescence at 495 nm which has long been established as being due to the deexcitation of Mn^{2+} ions.

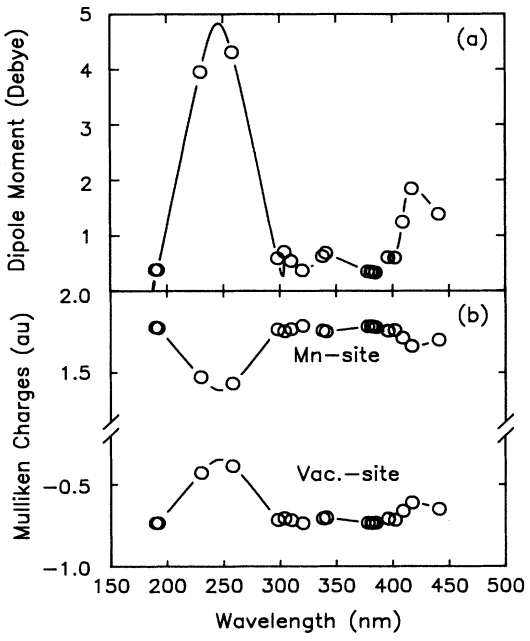

FIG. 7. Some calculated properties of the Mn-perturbed F-center cluster indicating the degree of charge transfer associated with the excited states. The cluster dipole moment (a) and the effective charges on the Mn and vacancy sites (b) are displayed as a function of the excitation wavelength. The excited-state energies and transition wavelengths are listed in Table I.

To better visualize the charge distortions involved in the transitions and especially the $3d$(c) transitions, we calculated for each state the cluster dipole moment and the effective charges at the Mn and vacancy sites using the Mulliken population analysis. The results are displayed in Fig. 7 as a function of excitation wavelength. Since the cluster is not symmetric about the vacancy one expects a nonzero cluster dipole moment for all the states. As Fig. 7(a) shows, the dipole moment is significantly greater in the 240 to 290 nm range, that is, for the $3d$(c) states. Figure 7(b) shows that this is the result of a shifting of charge onto the Mn site at the expense of charge in the vacancy. This observation lends support to those of Allen and McKeever[12] and Chakrabarti *et al.*,[50] who argue that optical bleaching at these wavelengths releases excited F centers from Mn-perturbed F-center complexes.

C. *F*-center transitions and the 540 nm peak

The final set of states arise primarily from excitations within the vacancy. These spin-2 and -3 F-center transitions both occur over the narrow range of 190 to 193 nm and correspond closely to peak structure over this same interval. Based on this evidence, we assign the peak centered at approximately 195 nm as resulting from spin-2 and -3 F-center transitions occurring within Mn/F defects. These results are somewhat surprising considering the fact that the F band in undoped CaF_2 occurs at 376 nm.[27] The exchange interaction with the neighboring Mn^{2+} $3d$ electrons thus represents a very significant perturbation to the F-center excited states.

Finally, we return to the issue of the 540 nm peak. From the CASSCF results obtained in this investigation, the 540 nm peak cannot be associated with transitions arising from the Mn/F defect. This peak, therefore, must be the result of transitions occurring within other defect complexes which may be created in CaF_2:Mn as a result of exposure to radiation. These defects must be thermally or optically removed in the same fashion as the Mn-perturbed F-center defect. This observation would indicate that an F-center-type defect is involved. Numerous possibilities exist such as clusters of F centers or clusters of Mn-perturbed F-centers. Optical absorption data for CaF_2:Mn for various doping levels ranging from undoped to 3% show a distinct shifting of the 540 nm peak toward shorter wavelengths as the Mn concentration is increased.[11] For undoped samples, this peak appears centered at 600 nm and shifts to 540 nm at 3% Mn concentration. Earlier absorption measurements for undoped samples correlate the existence of a peak at approximately 600 nm with the presence of defects consisting of two adjacent F centers (M centers).[27] It is important to note

that the samples used for the experimental data considered in this study were doped with Mn at levels approaching 3%. Although we do not present the results of calculations on the Mn-perturbed M center, it is conceivable that the absorption peak at 600 nm occurring in undoped samples for the M center could be shifted to 540 nm by a Mn perturbation. We therefore propose that the 540 nm absorption peak in Fig. 6 is due to ground- to excited-state transitions of Mn-perturbed M centers.

If this model is true, the reason the 540 nm peak anneals over the same temperature range as the Mn-perturbed F-center peaks is that the same processes that would lead to the breakup of the Mn/F defects, such as the release and diffusion of excited F centers (proposed by McKeever and Allen[12] and by Chakrabarti *et al.*[50] to explain TL, phototransferred TL, and optically stimulated luminescence), would also produce the breakup of M centers or Mn-perturbed M centers.

V. SUMMARY

The purpose of this paper was to analyze the complex changes in the absorption spectra of the Mn impurity in CaF_2:Mn following irradiation. In this study we have focused on the Mn/F defect that consists of an F center adjacent to a substitutional Mn^{2+} ion impurity. The electronic structure of this defect has been determined through CASSCF calculations on the embedded $[MnCa_3F_6Vac]^{1+}$ cluster. This cluster was chosen primarily by the need to surround the F center by ions that are treated quantum mechanically. Since four of the Mn^{2+} nearest-neighbor fluorines lie in the external lattice of this cluster, a study was made to determine the effects on the transition energies of the Mn^{2+} when no F center is present. The results show the effects to be minor (<0.1 eV), and demonstrate the adequacy of the approximations inherent in this choice of cluster and embedding potential.

Ultimately, the theoretical justification for any choice of cluster and/or computational method rests in its ability to predict the experimentally observed transitions from the calculated results. Our results show that not only do the embedded CASSCF calculations using this cluster produce transition energies that are in reasonably good agreement with the observed absorption spectrum, but the calculated Mn d-to-d transitions are in good agreement with those obtained from similar CASSCF calculations of the Mn d-to-d transitions for the O_h symmetry eightfold coordinated isolated Mn cluster recently investigated by the authors.[18] With slight perturbations, the same three bands of d-to-d transitions occur in both cases. The ground state of this defect was found to be spin 2. Thus the main effect of the adjacent F center is to make the d-to-d transitions spin allowed and to introduce additional states relating to transitions occurring within the vacancy. Our calculations further show that the important peak at 540 nm is not associated with this defect. We have proposed that it may be associated with Mn-perturbed M centers. While theoretical calculations for this defect were not carried out in this study, future embedded cluster CASSCF calculations could be used to verify this hypothesis.

ACKNOWLEDGMENTS

The authors wish to express their gratitude to S. W. S. McKeever and R. F. Wood for many helpful discussions. We would like to thank Konrad Brandermuhl at the Oklahoma State University Computer Center for his generous assistance throughout this work. This work was funded in part by the Naval Surface Warfare Center under Contract No. N60921-89-Q-10-137 and by U.S. Department of Education Grant No. P-200-A-900-59.

*Present address: Naval Surface Warfare Center, Code 682, White Oak Site, Silver Spring, Maryland 20903.

[1]R. J. Ginther and R. D. Kirk, J. Electrochem. Soc. **104**, 365 (1957).
[2]J. H. Schulman, F. H. Attix, E. J. West, and R. J. Ginther, Rev. Sci. Instrum. **31**, 1263 (1960).
[3]J. H. Schulman, in *Proceedings of the Symposium on Solid State and Chemical Radiation and Dosimetry in Medicine and Biology*, edited by J. H. Schulman (IAEA, Vienna, 1967), p. 3.
[4]J. H. Schulman, R. J. Ginther, S. G. Gorbics, A. E. Nash, E. J. West, and F. H. Attix, Int. J. Appl. Radiat. Isot. **20**, 523 (1969).
[5]A. C. Lucas and B. M. Kapsar, Health Phys. **27**, 600 (1974).
[6]S. W. S. McKeever, *Thermoluminescence of Solids* (Cambridge University Press, Cambridge, 1985), Chap. 6.
[7]Y. S. Horowitz, *Thermoluminescence and Thermoluminescent Dosimetry* (CRC, Boca Raton, FL, 1984), Vol. I, Chap. 4.
[8]R. Alcalá, P. J. Alonso, G. Lalinde, and A. Carretero, Phys. Status Solidi B **98**, 315 (1980).
[9]P. J. Alonso, V. M. Orera, and R. Alcalá, Phys. Status Solidi B **99**, 585 (1980).
[10]D. W. McMasters, B. Jassemnejad, and S. W. S. McKeever, J. Phys. D **20**, 1182 (1987).
[11]S. W. S. McKeever, B. Jassemnejad, J. F. Landreth, and M. D. Brown, J. Appl. Phys. **60**, 1124 (1986).
[12]P. Allen and S. W. S. McKeever, Radiat. Prot. Dosim. **33**, 19 (1990).
[13]P. J. Alonso and R. Alcalá, J. Lumin. **22**, 321 (1981).
[14]J. F. Rhodes, R. J. Abbundi, D. Wayne Cooke, V. K. Mathur, and M. D. Brown, Phys. Rev. B **31**, 5393 (1985).
[15]P. J. Alonso and R. Alcalá, J. Lumin. **21**, 147 (1980).
[16]D. Wayne Cooke, Evangelos P. Gavathas, and M. D. Brown, J. Appl. Phys. **54**, 1165 (1983).
[17]B. Jassemnejad, R. J. Abbundi, M. D. Brown, and S .W. S. McKeever, Phys. Status Solidi A **108**, 753 (1988).
[18]A. C. Lewandowski and T. M. Wilson, Phys. Rev. B **50**, 2780 (1994).
[19]W. A. Sibley and N. Koumvakalis, Phys. Rev. B **14**, 35 (1976).
[20]W. A. Sibley and N. Koumvakalis, J. Phys. C **10**, 4909 (1977).
[21]L. A. Kappers, S. I. Yun, and W. A. Sibley, Phys. Rev. Lett. **29**, 943 (1972).
[22]W. A. Sibley, S. I. Yun, and L. N. Feuerhelm, J. Phys. (Paris) Colloq. **34**, C9-503 (1973).
[23]S. I. Yun, K. H. Lee, W. A. Sibley, and W. E. Vehse, Phys. Rev. B **10**, 1665 (1974).
[24]W. E. Vehse and W. A. Sibley, Phys. Rev. B **6**, 2443 (1972).

[25]W. A. Sibley, S. I. Yun, and W. E. Vehse, J. Phys. C **6**, 1105 (1973).
[26]M. J. Frisch, G. W. Trucks, M. Head-Gordon, P. M. W. Gill, M. . . Wong, J. B. Foresman, B. G. Johnson, H. B. Schlegel, M. A. Robb, E. S. Replogle, R. Gomperts, J. L. Andres, K. Raghavachari, J. S. Binkley, C. Gonzalez, R. L. Martin, D. J. Fox, D. J. Defrees, J. Baker, J. J. P. Stewart, and J. A. Pople, GAUSSIAN 92 (Gaussian Inc., Pittsburgh, PA, 1992).
[27]*Crystals with the Fluorite Structure,* edited by W. Hayes (Oxford University Press, Oxford, 1974).
[28]R. F. Wood and T. M. Wilson, in *Defects in Insulating Solids,* edited by V. M. Tuchkevich and K. K. Shvarts (Springer-Verlag, Berlin, 1981), pp. 186–206.
[29]J. M. Vail, J. Phys. Chem. Solids **51**, 589 (1990).
[30]J. M. Vail, R. Pandey, and A. B. Kunz, Rev. Solid State Sci. **5**, 241 (1991).
[31]A. C. Lewandowski and T. M. Wilson (unpublished).
[32]J. M. Vail and C. Woodward, J. Phys. C **21**, 3901 (1988).
[33]O. E. Taurian and A. H. Tang Kai, J. Phys. Chem. Solids **47**, 65 (1986).
[34]S. Wilson, Adv. Chem. Phys. **69**, 439 (1987).
[35]S. Huzinaga, J. Andzelm, M. Klobukowski, E. Radzio-andzelm, Y. Sakai, and H. Tatewaki, *Gaussian Basis Sets for Molecular Calculations* (Elsevier, Amsterdam, 1984).
[36]A. B. Kunz and J. M. Vail, Phys. Rev. B **38**, 1058 (1988); A. B. Kunz, J. Meng, and J. M. Vail, *ibid.* **38**, 1064 (1988).
[37]D. R. Hartree, W. Hartree, and B. Swirles, Philos. Trans. R. Soc. A **238**, 229 (1939).
[38]B. O. Roos, P. R. Taylor, and P. E. M. Siegbahn, Chem. Phys. **48**, 157 (1980).
[39]J. Olsen, D. L. Yeager, and P. Jørgensen, Adv. Chem. Phys. **54**, 1 (1983).
[40]B. O. Roos, Adv. Chem. Phys. **69**, 399 (1987).
[41]R. Shepard, Adv. Chem. Phys. **69**, 63 (1987).
[42]H.-J. Werner, Adv. Chem. Phys. **69**, 1 (1987).
[43]I. Shavitt, Int. J. Quantum Chem. S **12**, 5 (1978).
[44]D. Hegarty and M. A. Robb, Mol. Phys. **38**, 1795 (1979).
[45]R. H. A. Eade and M. A. Robb, Chem. Phys. Lett. **83**, 362 (1981).
[46]E. A. Hylleraas and B. Undheim, Ann. Phys. (Leipzig) **65**, 759 (1930).
[47]J. K. L. MacDonald, Phys. Rev. **43**, 830 (1933).
[48]J. W. Richardson and G. J. M. Janssen, Phys. Rev. B **39**, 4958 (1989).
[49]M. Flórez, L. Seijo, and L. Pueyo, Phys. Rev. B **34**, 1200 (1986).
[50]K. Chakrabarti, J. Sharma, V. K. Mathur, and J. H. Barkyoumb, Phys. Rev. B **52**, 16 541 (1995).
[51]D. A. Patterson and R. G. Fuller, Phys. Rev. Lett. **18**, 1123 (1967).